

Slow relaxations and history dependence of the transport properties of layered superconductors

Raphaël Exartier¹ and Leticia F. Cugliandolo^{2*}

¹ *Laboratoire des Milieux Désordonnés et Hétérogènes, Tour 13 - case 86, 4 place Jussieu, F-75252 Paris Cedex 05, France*

² *Laboratoire de Physique Théorique de l'Ecole Normale Supérieure, 24 rue Lhomond, 75231 Paris Cedex 05, France and Laboratoire de Physique Théorique et Hautes Energies, Jussieu, 1er étage, Tour 16, 4 Place Jussieu, 75252 Paris Cedex 05, France*

(November 1, 2018)

We study numerically the time evolution of the transport properties of layered superconductors after different preparations. We show that, in accordance with recent experiments in $\text{Bi}_2\text{Sr}_2\text{CaCu}_2\text{O}_8$ performed in the second peak region of the phase diagram (Portier *et al.*, 2001), the relaxation strongly depends on the initial conditions and is extremely slow. We investigate the dependence on the pinning center density and the perturbation applied. We compare the measurements to recent findings in tapped granular matter and we interpret our results with a rather simple picture.

The behavior of the flux-line array in type II superconductors is determined by two competing interactions, the vortex-vortex repulsion that favors order in the form of a hexagonal lattice, and the attraction between vortices and randomly placed pinning centers due to material defects that, as thermal fluctuations, favors disorder. This competition generates a very rich static phase diagram [1]. More recently, the evolution of the spatial ordering of vortices driven out of equilibrium by, e.g., an external current has been analyzed analytically [2], numerically [3] and experimentally [4].

However, even in the absence of an external force, vortex systems show very rich nonequilibrium phenomena. Indeed, a hallmark of vortex dynamics is its history dependence. A vortex structure prepared by zero-field cooling (ZFC), in which the magnetic field is applied right after crossing the transition temperature, is expected to be more ordered than the one prepared by field cooling (FC), in which the magnetic field is applied before going through the transition [5–7] (see, however, [8]). Subsequently, thermal fluctuations allow for the rearrangement of the initial configurations. Studies of the evolution after FC and ZFC preparations of low- T_c and high- T_c type II superconductors have been performed with a variety of techniques that we non exhaustively summarize below.

The initial current ramp in the IV characteristic of a FC 2H-NbSe₂ sample has a large hysteretic critical value, suggesting that vortices are strongly pinned [6,7]. Once the flux lines are depinned, and one applies a subsequent ramp, the critical current takes a smaller value. In ZFC samples the critical current in both ramps is small [6]. The presence of metastability and hysteresis depends on the speed of the current ramp imposed to the system [9]. The ac response and complex resistivity in 2H-NbSe₂ also show that the FC state is strongly pinned and disordered while the ZFC state is not [7]. Similar effects have been exhibited in high T_c superconductors. For instance, Josephson plasma resonance experiments in $\text{Bi}_2\text{Sr}_2\text{CaCu}_2\text{O}_8$ (BSCCO) suggest that the

resonant field in FC samples is stationary while in ZFC samples it approaches the FC value asymptotically [10]. Still, thermomagnetic history effects in the solid vortex phase of pure twinned $\text{YBa}_2\text{Cu}_3\text{O}_7$ single crystals have been recently observed in ac susceptibility measurements [11]. On the numerical side, Olson *et al* studied how the fixed drive induced velocity (voltage response) depends upon time after different sample preparations, close to the order (3D) - disorder (2D) transition [12], focusing on the effect of superheating or supercooling the ordered and disordered phases [13].

In this Letter we concentrate on a recent study of the long-time transport properties of BSCCO monocystals after different preparations [14]. The experimental protocol is as follows. The same working conditions, given by a temperature $T = 4.5\text{K}$ and a magnetic field, $\mu_o H = 1.5T$, perpendicular to the c -axis are initially attained via a FC or a ZFC procedure. These values fall in the second peak region [6]. After a waiting-time $t_w = 30\text{min}$ a triangular pulse of current of duration $\tau_p \sim 10\mu\text{s} - 500\mu\text{s}$ is applied and an IV characteristic is recorded. During a second waiting period of the same duration t_w the sample is let freely evolve driven only by thermal fluctuations. The same external current is then applied and a second IV characteristic is recorded. This procedure is repeated so on and so forth. The first observation is that the shape of the IV loop changes as time elapses. In order to quantify its change, Portier *et al* chose a threshold tension, V_{TH} , defined the threshold current, I_{TH} , as the corresponding intensity in the IV characteristics, and monitored the dependence of I_{TH} on the discrete times $t_n = n(t_w + \tau_p)$, $n = 0, 1, \dots$. I_{TH} slowly relaxes in time, in a way that depends on the history of the sample. In the FC sample, after a seemingly static period that lasts until $t \approx 10^4\text{s}$, I_{TH} relaxes $\approx 25\%$ of its initial value over one decade in time, with a logarithmic decay. In the ZFC sample instead, I_{TH} smoothly increases by less than a tenth of its initial value over 6 decades. The asymptotic value of I_{TH} is the same for

both cooling procedures. The samples evolves in very long time scales, of the order of days.

The microscopic interpretation of experiments that probe the flux motion via the measurement of transport properties is not always straightforward. We reproduced the latter experiment with numerical simulations using a model of pancake vortices in a layered superconductor that successfully captures many of the observed effects in type II superconductors [12,15–19]. For adequately chosen sets of parameters our results are in qualitative accord with the measurements of Portier *et al* [14]. The advantage of using numerical simulations is twofold. First, it allows us to simply explore the effect of the microscopic parameters in the model. Second, it allows us to grasp what vortices are actually doing by direct visualization.

The model takes into account the long-range magnetic interactions between all pancakes. Since a flux line is essentially massless [1] we use overdamped Langevin dynamics. The equation of motion for a pancake located at a position $\mathbf{R}_i = (\mathbf{r}_i, z_i) = (x_i, y_i, z_i)$, ($\mathbf{z} \equiv \hat{c}$), is

$$\eta \frac{d\mathbf{r}_i}{dt} = \sum_{j \neq i} \mathbf{F}_v(r_{ij}, z_{ij}) + \sum_p \mathbf{F}_p(r_{ip}) + \mathbf{F}, \quad (1)$$

where $r_{ij} = |\mathbf{r}_i - \mathbf{r}_j|$ and $z_{ij} = |z_i - z_j|$ are the in-plane and inter-plane distances between pancakes i and j . η is the friction coefficient. The driving force per unit length due to an in-plane current \mathbf{J} acting on a vortex is $\mathbf{F} = \Phi_0 \mathbf{J} \times \hat{\mathbf{z}}$, with Φ_0 the quantum of magnetic flux. Quenched random point disorder is modeled by pinning centers that occupy uncorrelated random positions, taken from a uniform distribution, on each layer. They exert an attractive force on the vortices,

$$\mathbf{F}_p(r_{ip}) = -\frac{2A_p}{a_p^2} e^{-(r_{ip}/a_p)^2} \mathbf{r}_{ip}, \quad (2)$$

where A_p measures the amplitude of this force, a_p is the pinning range and $r_{ip} = |\mathbf{r}_i - \mathbf{r}_p|$ is the in-plane distance between vortex i and a pinning site at $\mathbf{R}_p = (\mathbf{r}_p, z_i)$. The magnetic interaction between pancakes is

$$\mathbf{F}_v(r, 0) = \frac{A_v}{r} \left[1 - \frac{\lambda_{||}}{\Lambda} \left(1 - e^{-r/\lambda_{||}} \right) \right], \quad (3)$$

$$\mathbf{F}_v(r, z) = -s \frac{\lambda_{||}}{\Lambda} \frac{A_v}{r} \left[e^{-|z|/\lambda_{||}} - e^{-R/\lambda_{||}} \right], \quad (4)$$

with $R = \sqrt{z^2 + r^2}$, $\Lambda = 2\lambda_{||}^2/d$ the 2D thin-film screening length, d the inter-layer spacing and $\lambda_{||}$ the in-plane penetration length. One can vary the relative strength of the interlayer coupling by tuning the prefactor s [12,16,18]. The model in Eqs. (3) and (4) is valid in the limit $d \ll \lambda_{||} \ll \Lambda$ [20]. We normalize length scales by $\lambda_{||}$, energy scales by $A_v = \Phi_0^2/4\pi^2\Lambda$ and time by $\tau = \eta\lambda_{||}^2/A_v$, that for BSCCO yields $\tau \sim 1\mu\text{s}$. We consider N_v vortices and N_p pinning centers per layer in N_l rectangular layers of size $L_x \times L_y$ ($L_x = \sqrt{3}/2L_y$). The normalized vortex

density is $n_v = B/\Phi_0 = N_v/(L_x L_y)$. Following [15] we consider $n_v = 0.12$, $A_p/A_v = 0.2$, $a_p = 0.1$, $d = 0.01$ and $\Lambda = 200$ which correspond to BSCCO [20]. We use $N_v = 25$ vortices in up to $N_l = 4$ layers. The value of a_p as compared to n_p is of first importance and will be discussed later on. We use periodic boundary condition in all directions and the periodic long-range in-plane interaction is evaluated with an exact and fast converging sum [17]. All the simulations are at $T = 0$, with a time-step 0.01, and averaged over 90 realizations.

We mimic the external current applied with an increasing (in steps) force \mathbf{I} parallel to the x axis. It results in an average motion of the pancakes, with velocity $V = [\langle V_x(t) \rangle] = (N_v N_l)^{-1} \sum_i [\langle dx_i/dt \rangle]$. (The angular and square brackets represent an average over different realizations of the dynamics and disorder, respectively.) We match the notations in Ref. [14] by calling I_{TH} the value of the applied force which leads to an average speed equal to a previously chosen threshold V_{TH} . We have checked that the results do not depend qualitatively on the precise value of V_{TH} , if *e.g.* $V_{\text{TH}} \leq 0.2$ for $I_{\text{MAX}} = 1.4$ and $n_p = 0.25$.

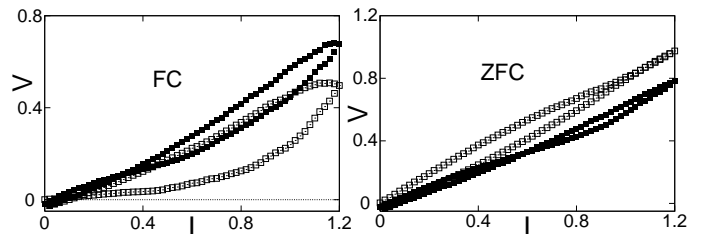


FIG. 1. Current-voltage curves at times $t_1 = 0$ (open circles) and $t_2 = 20$ (filled circles) for a monolayer of pancake vortices with $n_p = 0.12$, $t_w = 6$, $\tau_p = 14$ and $I_{\text{MAX}} = 1.2$.

Experimentally, vortices are created on the surface of the sample when the magnetic field is turned on. It happens during cooling for FC samples and later for ZFC samples. Afterwards, they penetrate the sample and new ones are created on the border. This procedure is difficult to implement in this model. We differentiate the FC and ZFC initial states by choosing different initial repartitions of vortices. For the FC samples, we choose an initial condition with each vortex pinned to a defect, in which the distance to the nearest pinning center is less than the pinning range a_p . To reproduce the ZFC samples, we choose an ordered hexagonal lattice [5–7]. This procedure neglects the critical state and it is expected to describe the behavior in the bulk.

In Fig. 1 we display the first two IV loops for a 2D system that starts from a pinned (FC) or hexagonal (ZFC) initial condition. As expected [9,19], the first ramp shows hysteresis and a large critical current for the FC sample. In the second ramp the loop moves and it is partially closed. The ZFC sample has a much lower critical current (that may even vanish). The pulse we used is as

fast as the fastest used experimentally, $\tau_p = 14$ in real time; consequently, the critical currents are very weak. Moreover, since the waiting-time between two successive pulses is here $t_w \sim \tau_p$, while in [14] $t_w \gg \tau_p$, we are perturbing the system in a much stronger manner than done experimentally. By the end of this Letter we shall study the dynamics under a less invasive probe.

The time-dependence of the IV loop is quantified in Fig. 2-left where we show the evolution of I_{TH} against t_n for two n_p . The curves correspond to pinned (open circles) and hexagonal (filled squares) initial conditions. The first two points in the lower curves for the pinned and hexagonal initial conditions correspond to the IV curves in Fig. 1. There is an initial fast motion that translates into a rather fast drop in $I_{\text{TH}}^{\text{FC}}$ and a fast increase of $I_{\text{TH}}^{\text{ZFC}}$. Later, the curves approach their common asymptote in a slower than exponential manner. The qualitative behavior of these curves resembles the ones in [14] though with much shorter relaxation times.

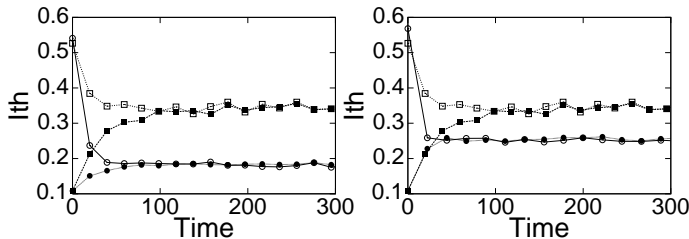


FIG. 2. Left: The threshold current $I_{\text{TH}}(t_n)$ against time in a monolayer with $n_p = 0.12, 0.25$ (upper to lower asymptotic value). Open symbols: pinned, FC; filled symbols: lattice, ZFC. $I_{\text{MAX}} = 1.4$. Right: $I_{\text{TH}}(t_n)$ for $I_{\text{MAX}} = 1.4$, $\tau_p = 14$, $t_w = 6$ (above) and $I_{\text{MAX}} = 1.6$, $\tau_p = 26$, $t_w = 4$ (below). FC (open symbols) and ZFC (filled symbols). $n_p = 0.25$.

A closer inspection of the model and procedure suggests that the precise shape of these curves may depend on several parameters like n_p , the form of the ramp and the choice of the sequence t_n . For very small values of n_p no interesting effect is expected since there are not enough pinning centers to stop the vortices. For intermediate densities, *e.g.* $n_p = 0.12$, we found the curves in Fig. 2-left. The asymptotic value of $I_{\text{TH}}(t_n)$ increases with n_p . Eventually, if n_p is so large that the distance between pinning centers is smaller than the range of the pinning force, *i.e.* $n_p > \pi^{-1}(2a_p)^{-2}$, there is no difference between ZFC and FC preparations and after a very few iterations the two curves collapse.

The maximum intensity in the ramp, I_{MAX} , is also an important parameter. The asymptotic value of $I_{\text{TH}}(t_n)$ decreases with I_{MAX} . For a stronger I_{MAX} , *e.g.* $I_{\text{MAX}} = 1.6$ in Fig. 2-right, the memory of the initial condition is very quickly lost since the vortices are pushed too strongly by the force. The perturbation itself, *i.e.* the sequence of current/force pulses, is driving the system to different steady states characterized by $I_{\text{TH}}(t_n \rightarrow \infty)$.

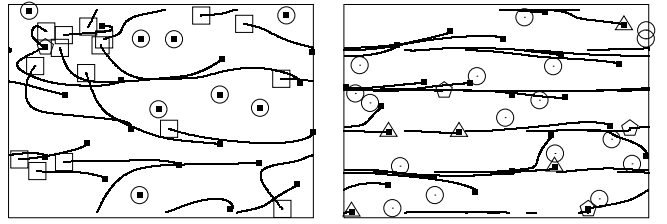


FIG. 3. Vortex trajectories of the FC (left) and ZFC (right) samples during the first pulse (lines). Pinning centers where a vortex gets pinned are represented with triangles, those from which a vortex depins are represented with squares and those where vortices get pinned and later depin are represented with pentagons. Pinning centers unaffected by the pulse (whether there is a vortex permanently pinned to them or not) are represented with circles.

Analyzing the motion of vortices during each pulse helps us understanding these results. During the first pulse a fraction of vortices in the FC sample remains pinned while the rest rapidly depin and move in the sample. How many of them depin depends on τ_p and I_{MAX} . On the left of Fig. 3 we display the vortex trajectories with lines and the positions of pinning centers with symbols; 15 vortices move while the rest remain pinned. Some trajectories join two pinning centers. During the quiescent time t_w a number of vortices may get again pinned, depending on n_p , the strength of the different interactions and thermal fluctuations. In the second pulse new vortices depin and, consequently, I_{TH} decreases.

Instead, the initially ordered sample rapidly reaches a smectic flow [2] (Fig. 3-right). During this moving period, the vortices that move close to pinning centers get pinned; other vortices are pulled by the force and depin, but get later pinned by another pinning center. By the end of the first ramp, the hexagonal lattice has been deformed and 6 vortices are pinned. At $T = 0$ the displacement during the quiescent time t_w is rather small. This mechanism repeats in subsequent periods and the threshold intensity increases in time. This picture is confirmed by the study of the position of each vortex relative to its closest pinning center as a function of t_n . In the initially pinned sample, on average and in time, vortices move away from the pinning centers. In an initially depinned sample, vortices get pinned by a pinning center. A Delaunay triangulation analysis shows that at long times, *e.g.* $t_n = 1500$, both initially ordered and pinned systems become a deformed hexagonal lattice.

We wish to check if this is a plausible explanation of the results in [14]. Certainly, we have almost continuously stirred the sample while the probing pulses applied experimentally, being widely separated in time, are much weaker. Unfortunately we cannot match the experimental conditions $t_w \gg \tau_p$ ($t_w = 30\text{min} \equiv 10^9$ iterations!). On the other hand, mechanical vibrations have not been totally eliminated from the experiment and might induce an important supplementary means for relaxation [14].

Another important difference between our numerical study and the experiment in [14] is that we have worked at $T = 0$ (with the aim of reducing the thermal noise and improving the averaging) while experiments are done at low but non-vanishing T . The $T = 0$ protocol is very close to the ones used to probe the dynamics of granular matter. Indeed, temperature is totally irrelevant in these systems and the rearrangement of grains is induced by pumping energy in the sample in, e.g., the form of periodic taps [21]. If the vortex system at $T = 0$ behaves as granular matter, all the dynamics must then take place during the probing pulses while the systems should be essentially static in a metastable configuration during t_w . In Fig. 4 we analyse the dependence of the relaxation time-scale on t_w by comparing $I_{\text{TH}}^{\text{FC,ZFC}}(t_n)$ for $t_w = 3, 144, 288$ and $\tau_p = 14.4$ in all cases. The longer t_w the slower the approach to the asymptotic value. The inset shows I_{TH} against the number of perturbing cycles n . The three curves now collapse showing that at $T = 0$ the evolution of I_{TH} takes place during τ_p and it is almost completely due to the perturbation. It would be very interesting to check if this also happens experimentally.

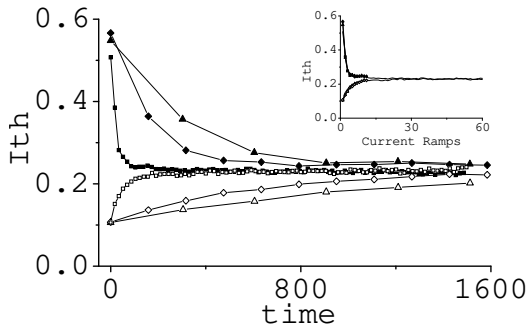


FIG. 4. The threshold intensity against time for FC (filled symbols) and ZFC (open symbols) preparations and $t_w = 3, 144, 288$, $\tau_p = 14.4$ (circles, diamonds, triangles). In the inset, the same curves are plotted in function of the number of current ramps applied and they rescale perfectly.

The mechanism for the very slow relaxation in the experimental system may be the one put forward in the previous paragraph. The relaxation of the FC and ZFC samples are controlled by the parameters in the model (n_p , I_{MAX} , etc). Hence, by changing the values of the parameters, one can explain the difference in the experimental observations described in the introduction. We have also simulated 3D systems with different number of layers (1 to 4) and interlayer coupling strengths s (1 to 9), and observed no qualitative difference in the I_{TH} relaxation though its time-scale increases considerably.

We wish to thank very useful discussions with P. Chauve, F. De la Cruz, G. d'Anna, D. Dominguez, T. Giamarchi, A. Kolton, P. Le Doussal, S. Valenzuela and especially F. Portier and F. Williams for communicating their results to us prior to publication, and continuous

discussions during this work.

* ICTP Research Staff Associate.

- [1] G. Blatter *et al*, Rev. Mod. Phys. **66**, 1125 (1994). T. Giamarchi and P. Le Doussal, *Statics and dynamics of disordered elastic systems*, in Spin glasses and random fields, A.P. Young ed. (World Scientific, 1997). T. Nattermann and S. Scheidl, Adv. Phys. **49**, 607 (2000).
- [2] T. Giamarchi and P. Le Doussal, Phys. Rev. Lett. **76** 3408 (1996). L. Balents, M. C. Marchetti and L. Radzihovskiy, Phys. Rev. **B57**, 775 (1998). P. Le Doussal and T. Giamarchi, Phys. Rev. **B57**, 11356 (1998). S. Scheidl and V. M. Vinokur, Phys. Rev. **E57**, 2574 (1998).
- [3] A. E. Koshelev and V. M. Vinokur, Phys. Rev. Lett. **73**, 3580 (1994). M. C. Faleski, M. C. Marchetti and A. A. Middleton, Phys. Rev. **B54**, 12427 (1996). K. Moon, R. T. Scalettar and G. T. Zimanyi, Phys. Rev. Lett. **77**, 2778 (1996). C. J. Olson, C. Reichhardt and F. Nori, Phys. Rev. Lett. **81**, 3757 (1998). A. B. Kolton, D. Domínguez and N. Gronbech-Jensen, Phys. Rev. Lett. **83**, 3061 (1999). H. Fangohr, unpublished.
- [4] M. Marchevaky *et al*, Phys. Rev. Lett. **78**, 531 (1997). F. Pardo *et al.*, Nature **396**, 348 (1998). A. M. Troyanovskiy, J. Aarts and P. H. Kes, Nature **399**, 665 (1999).
- [5] P. H. Kes and C. C. Tsuei, Phys. Rev. **B28**, 5126 (1983).
- [6] W. Henderson *et al.*, Phys. Rev. Lett. **77** 2077 (1996). N. R. Dilley *et al* Phys. Rev. **B56**, 2379 (1997). E.Y. Andrei *et al* J. Phys. IV, **10** (1999) 5.
- [7] W. Henderson *et al.*, Phys. Rev. Lett. **81** (1998) 2353. G. Ravikumar *et al* Phys. Rev. **B58**, R11069 (1998). S. S. Banarjee *et al* Phys. Rev. **B58**, 995 (1998).
- [8] F. de la Cruz, M. Menghini and Y. Fasano, Physica C **341** (2000).
- [9] Z. L. Xiao *et al* Phys. Rev. Lett. **83**, 1664 (1999), *ibid* **85**, 3265 (2000), *ibid* **86**, 2431 (2001).
- [10] Yuji Matsuda *et al* Phys. Rev. Lett. **78**, 1972 (1997).
- [11] S. O. Valenzuela and V. Bekkeris, Phys. Rev. Lett. **84**, 4200 (2000), Phys. Rev. Lett. **86**, 504 (2001)
- [12] C. Olson *et al*, cond-mat/0004054 and cond-mat/0008350.
- [13] E. Zeldov *et al*, Nature **375**, 373 (1995). X. S. Ling *et al* Phys. Rev. Lett. **86**, 712 (2001).
- [14] B. Das *et al*, Phys. Rev. **B61**, 9118 (2000); F. Portier *et al* in preparation.
- [15] A. B. Kolton *et al*, Physica **C341-348**, 1007 (2000), Phys. Rev. Lett. **83**, 3061 (1999).
- [16] C. J. Olson and N. Grønbech-Jensen, cond-mat/0002064
- [17] N. Grønbech-Jensen, Comp. Phys. Comm. **119**, 115 (1999).
- [18] C. Olson *et al*, cond-mat/0006172.
- [19] C. J. Olson, C. Reichhardt and V. Vinokur, cond-mat/0010002.
- [20] J.R. Clem, Phys. Rev. B. **43**, 7837 (1991).
- [21] H. M. Jaeger, S. R. Nagel and R. P. Behringer, Rev. Mod. Phys. **68**, 1259 (1996).